Measurement of the intrinsic variability within protein crystals: implications for sample-evaluation and data-collection strategies

Michael G. Bowler[a] and Matthew W. Bowler[b,c]*

[a]Department of Physics, University of Oxford, Keble Road, Oxford OX1 3RH, England, [b]European Molecular Biology Laboratory, Grenoble Outstation, 6 Rue Jules Horowitz, 38042 Grenoble, France, and [c]Unit of Virus Host-Cell Interactions, Université Grenoble Alpes–EMBL–CNRS, 6 Rue Jules Horowitz, 38042 Grenoble, France

Correspondence e-mail: mbowler@embl.fr

The advent of micro-focused X-ray beams has led to the development of a number of advanced methods of sample evaluation and data collection. In particular, multiple-position data-collection and helical oscillation strategies are now becoming commonplace in order to alleviate the problems associated with radiation damage. However, intra-crystal and inter-crystal variation means that it is not always obvious on which crystals or on which region or regions of a crystal these protocols should be performed. For the automation of this process for large-scale screening, and to provide an indication of the best strategy for data collection, a metric of crystal variability could be useful. Here, measures of the intrinsic variability within protein crystals are presented and their implications for optimal data-collection strategies are discussed.

1. Introduction

In the last ten years, protein micro-crystallography (Cusack *et al.*, 1998; Riekel *et al.*, 2005) has moved from a highly unusual and specialized technique to a standard method in modern structural biology (Smith *et al.*, 2012). The large multi-component complexes and membrane proteins now routinely studied tend to produce either very small crystals or crystals that can be extremely heterogeneous in their diffraction properties. The increasing availability of micro-focused or micro X-ray beams (diameter < 10 μm; Flot *et al.*, 2010; Sanishvili *et al.*, 2008; Axford *et al.*, 2012) with experimental environments optimized for macromolecular crystallography has led to the evolution of advanced sample-evaluation and data-collection protocols, such as mesh scans and helical oscillations (Bowler *et al.*, 2010; Cherezov *et al.*, 2009; Flot *et al.*, 2010; Song *et al.*, 2007; Aishima *et al.*, 2010; Hilgart *et al.*, 2011). The ability of a microbeam to spread the effect of radiation damage across a larger volume of a crystal or to resolve the most ordered part of a crystal that is relatively larger than the beam size (Sanishvili *et al.*, 2008) has brought a much larger variety of samples to these beamlines (Flot *et al.*, 2010). In many of the most challenging projects it has proved essential, rather than advantageous, to be able to collect data from multiple positions or to use helical oscillations (Efremov *et al.*, 2010; Warne *et al.*, 2008). Recently, a number of automated procedures to define the best position within a crystal from which to collect data have been described (Bowler *et al.*, 2010; Sanishvili *et al.*, 2008; Song *et al.*, 2007; Aishima *et al.*, 2010; Hilgart *et al.*, 2011). However, a measure of the variability of diffraction quality within a crystal would provide an indication of the degree of homogeneity both within and between crystals of a certain macromolecule and could act as an initial guide to beamline choice and data-collection strategy. Here, metrics of the innate variability within crystals are presented. A number of systems, varying from large multi-component complexes to membrane proteins and small soluble proteins, have been tested. The values provide an initial measure of the extent of variability and could be used to indicate whether a large or small beam should be used and whether single-position or multiple-position strategies should be employed. As the level of automation and the number of samples requiring evaluation increases at synchrotron facilities in the future, automated pre-evaluation and measurement of variability will be essential in the selection of optimized data-collection facilities and strategies.
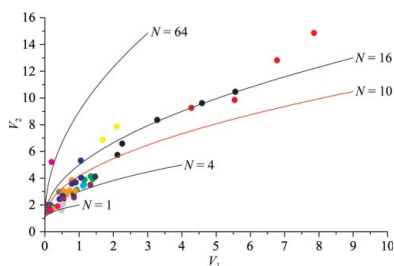
laboratory communications

Table 1
Sample information, scan parameters and measurements of the variation of diffraction quality for a number of crystals of macromolecules.

Sample	Sample size (max × min) (µm)	Beamline (beam diameter, µm)	No. of positions	V_1	V_2	h	N
RhoA data	350 × 50	ID23-2 (7)	1 (30°, 165-image data set)	0.02	1.36	–	–
F_1 data	200 × 50	ID23-2 (7)	1 (30°, 333-image data set)	0.02	1.60	–	–
p38	100 × 10	ID23-1 (20)	50 (mesh)	0.08	1.50	1.8	3.1
GPCR	300 × 10	ID23-2 (7)	90 (mesh)	0.15	1.66	2.1	2.9
Reverse transcriptase	300 × 100	ID23-1 (30)	42 (mesh)	0.17	1.57	2.2	1.9
Ribosome, small crystal	400 × 100	ID29 (20)	161 (line)	0.20	5.21	5.4	88.6
PGK	400 × 20	ID14-1 (100)	35 (mesh)	0.22	1.72	2.5	2.4
Ultralente insulin	20 × 20	ID23-1 (20)	200 (mesh)	0.25	1.83	2.6	2.6
Reverse transcriptase	100 × 50	ID23-1 (30)	42 (mesh)	0.38	1.89	3.3	2.1
Membrane-bound pyrophosphatase (PVP)	50 × 30	ID23-2 (7)	159 (mesh)	0.42	2.97	3.8	9.2
GPCR	300 × 10	ID23-2 (7)	90 (mesh)	0.43	2.43	3.4	4.8
Trypsin	800 × 100	ID14-1 (100)	20 (mesh)	0.49	1.59	9.4	0.7
GPCR	300 × 10	ID23-2 (7)	90 (mesh)	0.53	2.66	3.9	5.2
Trypsin	800 × 100	ID14-1 (100)	20 (mesh)	0.53	2.06	4.1	2.1
Ferulic acid esterase (FAE)	300 × 100	ID14-4 (50)	16 (mesh)	0.54	2.42	3.9	3.7
PGK	400 × 20	ID14-1 (100)	35 (mesh)	0.55	3.03	4.2	7.5
PGK	400 × 20	ID14-1 (100)	35 (mesh)	0.63	2.73	4.3	4.8
PGK	400 × 20	ID14-1 (100)	35 (mesh)	0.72	3.07	4.7	5.9
PGK	400 × 20	ID14-1 (100)	35 (mesh)	0.79	3.84	5.3	10.2
GPCR	300 × 10	ID23-2 (7)	90 (mesh)	0.79	3.58	5.2	8.4
PGK	400 × 20	ID14-1 (100)	35 (mesh)	0.82	3.66	5.3	8.6
p38 multiple crytals	100 × 10	ID23-1 (20)	40 (mesh)	0.84	2.79	5.3	3.8
FAE	300 × 100	ID14-1 (100)	25 (mesh)	0.85	2.56	5.6	2.9
PGK	400 × 20	ID14-1 (100)	35 (mesh)	0.89	3.04	5.4	4.7
GPCR	300 × 10	ID23-2 (7)	64 (mesh)	0.90	3.68	5.5	8.0
Glucose isomerase	50 × 30	ID23-1 (20)	64 (mesh)	0.93	3.12	5.6	4.8
GPCR	300 × 10	ID23-2 (7)	450 (mesh)	1.05	5.31	7.0	17.7
GPCR	300 × 10	ID23-2 (7)	90 (mesh)	1.06	4.03	6.2	8.7
Ribosome, large crystal	700 × 100	ID29 (20)	415 (line)	1.12	3.43	6.4	5.3
Glucose isomerase	50 × 30	ID23-1 (20)	64 (mesh)	1.14	3.52	6.4	5.6
Glucose isomerase	50 × 30	ID23-1 (20)	64 (mesh)	1.16	3.88	6.5	7.2
Ferulic acid esterase (FAE)	300 × 100	ID14-1 (100)	24 (mesh)	1.33	3.49	7.5	4.7
Glucose isomerase	50 × 30	ID23-1 (20)	64 (mesh)	1.34	4.13	7.2	7.3
Glucose isomerase	50 × 30	ID23-1 (20)	64 (mesh)	1.40	3.93	7.5	6.1
Thermolysin	500 × 50	ID29 (30)	45 (mesh)	1.47	4.11	7.8	6.6
Membrane-bound pyrophosphatase (TVP)	100 × 50	ID23-2 (7)	185 (mesh)	1.69	6.86	9.6	20.3
Membrane-bound pyrophosphatase (TVP)	100 × 50	ID23-2 (7)	160 (mesh)	2.10	7.86	11.3	22.4
RhoA	350 × 50	ID23-2 (7)	99 (mesh)	2.12	5.74	10.4	10.6
RhoA	350 × 50	ID23-2 (7)	98 (mesh)	2.26	6.57	11.1	13.7
RhoA	350 × 50	ID23-2 (7)	97 (mesh)	3.28	8.35	15.1	16.5
F_1-ATPase	200 × 50	ID23-2 (7)	238 (mesh)	4.28	9.25	19.2	15.9
RhoA	350 × 50	ID23-2 (7)	98 (mesh)	4.59	9.61	20.6	16.2
F_1-ATPase	200 × 50	ID23-2 (7)	230 (mesh)	5.54	9.84	26.4	14.1
RhoA	350 × 50	ID23-2 (7)	98 (mesh)	5.56	10.46	25.4	16.1
F_1-ATPase	200 × 50	ID23-2 (7)	238 (mesh)	6.78	12.81	30.1	20.6
F_1-ATPase	200 × 50	ID23-2 (7)	238 (mesh)	7.86	14.86	34.3	24.4

2. Experimental procedures and results

2.1. Crystal preparation

Crystals of bovine mitochondrial F_1-ATPase were grown as described previously (Lutter *et al.*, 1993), with the exception that azide and ADP were omitted from all buffers. The crystals were mounted on MicroMesh loops (MiTeGen, Ithaca, New York, USA) and conditioned with the HC1b humidity-control device (Sanchez-Weatherby *et al.*, 2009; Russi *et al.*, 2011; Wheeler *et al.*, 2012), using conditions previously established for maximum improvement of crystal diffraction properties (Bowler *et al.*, 2006).

Recombinant human RhoA crystals were grown, harvested on a MicroMesh (MiteGen, Ithaca, New York, USA) and cryocooled directly as described previously (Pellegrini *et al.*, 2011). Crystals of the closed conformation of β-phosphoglucomutase (β-PGM) from *Lactobacillus lactis* were grown as described previously (Baxter *et al.*, 2010; Griffin *et al.*, 2012). Crystals of thermolysin from *Bacillus thermoproteolyticus* were grown according to established protocols (Mueller-Dieckmann *et al.*, 2005). Crystals of human PGK were grown as described previously (Cliff *et al.*, 2010). Ultralente insulin (Ultratard, Novo Nordisk, Denmark) and glucose isomerase microcrystals (Sigma–Aldrich) were swept out of solution using a Micro-

Mesh (MiTeGen, Ithaca, New York, USA), excess liquid was removed and they were cryocooled directly (Pellegrini *et al.*, 2011).

All other crystals were provided by their owners for testing; particular thanks are due to Tony Warne and Venki Ramakrishnan (MRC Laboratory of Molecular Biology, Cambridge, England) for crystals of β_1-andregenic G-protein coupled receptor from turkey, prepared as described in Warne *et al.* (2008), and of the 70S ribosome from *Thermus thermophilus*, prepared as described in Selmer *et al.* (2006), respectively.

2.2. Mesh scans, line scans and data processing

Mesh scans were launched as described in Bowler *et al.* (2010) using the workflow interface in the *MXCuBE* beamline GUI (Brockhauser *et al.*, 2012; Gabadinho *et al.*, 2010). Briefly, a mesh is defined by drawing a box over the area of interest on the image from the beamline video microscope. The number of vertical and horizontal steps is then defined to produce a mesh where an image will be taken at the intersection of lines; here, the step size was similar to the beam diameter in order avoid overlapping areas. These points are converted to positions of the goniometer centring table and translation motors, and data collection is then performed at the corre-

sponding positions. Line scans are similar to mesh scans except that only two points are defined and the number of images to be collected between these points (the step size) is defined. Line scans were used when assessing the diffraction quality along needle-shaped crystals. Diffraction images were processed using an *EDNA* (Incardona *et al.*, 2009) characterization plugin running *labelit.distil* (Sauter *et al.*, 2004; Zhang *et al.*, 2006), *MOSFLM* (Powell *et al.*, 2013) and *BEST* (Bourenkov & Popov, 2010), producing a large number of metrics for the comparison of diffraction quality. The choice of metric for diffraction quality is not always obvious. Here, we have selected the total integrated signal above background (TIS) as the best way to measure variation within a crystal, as it provides a good measure of the differences in diffraction intensities. Other metrics, such as the number of spots, are also a good measure of the quality, but as the higher resolution spots are often missed, differences between positions may not be highlighted. Calculation of differences using the number of spots leads to a similar trend as for the total signal above background, but is less discriminating (data not shown). The calculations presented here are applicable to any measure of quality. The diameter of physically contiguous images with TIS values within 10% of each other was also output in order to give an indication of the area of the best regions. Images without diffraction, those containing ice rings or weak diffraction from 'glancing blows' were excluded from variability calculations by only including images with a number of counts above a threshold value.

2.3. Measuring intra-crystal variability

What is the best strategy for data collection? If a crystal diffracts homogenously then the best option is to match the beam size to the crystal and use the full diffraction power of the crystal and distribute the dose across a larger sample volume. If the quality of the crystal varies then the best strategy will be to use only the most ordered volumes. In this study, the diffraction characteristics of a large variety of samples has been probed with X-ray beams of varying size (Table 1), including a number of challenging projects where parti-

cular data-collection strategies using either large ($\geq$100 µm diameter) or small ($\leq$10 µm diameter) beams have already been shown to be essential. Nothing can replace an in-depth knowledge of crystals of a particular sample, but a metric of the extent of variability could be useful in providing an early indication of the level of homogeneity of samples for a particular project.

In order to provide a general definition of sample variability, a normalized value should be assigned in order to be comparable between samples and projects. Two measures present themselves: the variance divided by the square of the mean (1) and the peak value divided by the mean (2),

$$V_1 = \frac{\sum\limits_{k=1}^{n}(T_k - \overline{T})^2}{n - 1} \bigg/ [\overline{T}]^2, \tag{1}$$

$$V_2 = \frac{T_{\max}}{\overline{T}}, \tag{2}$$

where T_k is the TIS of a position within a crystal, $\overline{T}$ is the average TIS, $T_{\max}$ is the highest value of the TIS and n is the number of positions. For perfectly homogenous crystals $V_1 = 0$ as there will be no variation about the mean and $V_2 = 1$ as the peak will be equal to the mean.

Mesh and line scans were performed on a variety of samples and values of V_1 and V_2 were calculated (Table 1). The values were calculated for separate crystals, except for RhoA, where each value was calculated from a different orientation of the same crystal ($\omega = 0$, 30, 60, 90 and 120°). The values obtained vary considerably and, from knowledge of the samples studied, provide a good measure of the degree to which the diffraction quality varies within a crystal (Fig. 1). The values are highly correlated ($R^2 = 0.98$) and most crystals examined here have $V_1 < 2$ and $V_2 < 4$, which indicate a high degree of homogeneity. Could the variation in the calculated values arise from factors other than heterogeneity? An explanation for greater variability within some crystals could be that crystal size affects variability, either through increasing disorder or simply by an increase in the number of positions sampled. Plotting V_1 against crystal size shows
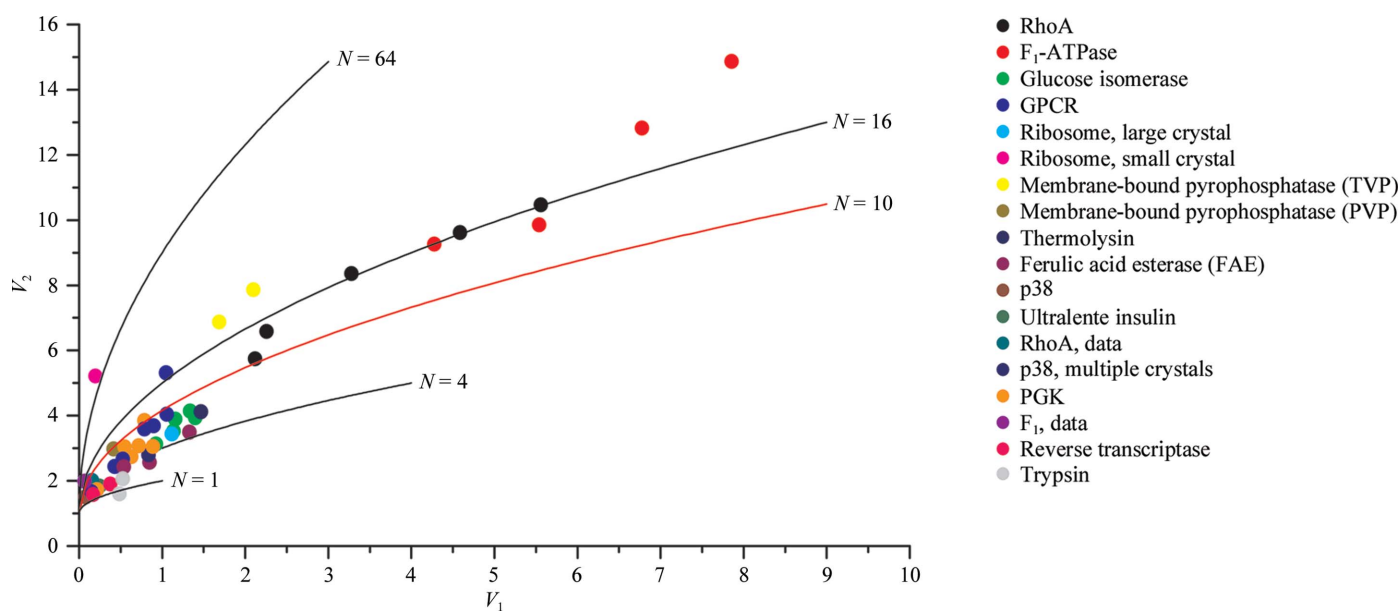

Figure 1
Comparison of variability measures of crystals. Values of V_1 and V_2 are plotted against each other and coloured according to sample type. Lines show the values obtained for various ratios N between positions at increasing differences in diffraction power (see §2.4 for an explanation of the model). The red line representing the ratio $N = 10$ is a reasonable cutoff between variable and homogenous diffraction within crystals.

the value does not necessarily increase with increasing crystal size (Fig. 2). As a further control, values of V_1 and V_2 were calculated for 30° angular ranges collected from single positions within the crystals with the highest observed values (F_1-ATPase and RhoA). The values obtained from these data sets ($V_1 = 0.02$ for both systems) show that the intensity of the diffraction images varies very little, even when collected over a rotation range (Table 1). This demonstrates that the values reasonably reflect the difference in diffraction quality between positions within a crystal.

2.4. Model calculations

Scanning a beam across a crystal yields a patchwork of TIS values corresponding to local variations in the quality of the crystal. As the variance has been normalized, the values of both V_1 and V_2 are characteristic only of the crystal and its orientation; these measures are independent of the beam intensity and allow comparison of different orientations and indeed different crystals. A large variance implies high local variability in crystal quality. Further insight can be gained by employing a model construct which, although limited, is nonetheless illuminating. If the variability of a given specimen were precisely known, V_1 and V_2 could be calculated (as could any other measure). As it is, these two measures can determine two numbers more obviously related to crystal variability, but only two. We suppose that each position in the mesh belongs to one of two classes. The lower class yields a TIS of magnitude 1 and the other class a magnitude $h > 1$. We suppose that the ratio of the number of positions of magnitude 1 to those of magnitude h is N. Thus, a crystal diffracting strongly from one local area will have a large value of h and a large value of N. From any given data set, the values of h and N in the simple equivalent model can be constructed. Given h and N, the values of V_1 and V_2 can be calculated; such an imaginary sample would yield (3) and (4),

$$V_1 = N \frac{(h-1)^2}{(h+N)^2}, \tag{3}$$

$$V_2 = h \frac{(N+1)}{(h+N)}. \tag{4}$$

These equations can be solved to yield the parameters h and N in terms of measured values of V_1 and V_2 (equations 5 and 6),

$$h = V_2 \frac{(V_2 - 1)}{(V_2 - 1 - V_1)}, \tag{5}$$

$$N = \frac{(V_2 - 1)^2}{V_1}. \tag{6}$$

Finally, either h or N can be eliminated, to give, for example, a relation between V_1 and V_2. If h is eliminated, the relation between V_1 and V_2 defines a curve for constant N, a measure of the variegation of the crystal (7),

$$V_2 = (N \times V_1)^{1/2} + 1. \tag{7}$$

Plots of values of V_1 and V_2 for ratios N of between 1 and 64 for increasing values of h are shown in Fig. 1. In different orientations the same crystal will approximately define such a curve when scanned in different orientations, as for RhoA, where the ratio of good regions to bad remains constant but h changes. The model curves provide an indication of how variation within a crystal is reflected in the values of V_1 and V_2. The most ordered systems fall below values that represent a ratio N of 10:1 (Fig. 1, red line). Crystals with higher variation (GPCR, pyrophosphatase, F_1-ATPase and RhoA) have ratios N

equivalent in the model to between 15:1 and 25:1 accompanied by large differences in diffraction intensity (h). The most striking is the small ribosome crystal, where a very large ratio is observed. The model demonstrates that the combination of both values is essential, as when a small number of good areas are present low V_1 can mask a high V_2.

Do the values relate to isomorphism between positions? The purpose of these values is to give an idea of the variation in intensity within a crystal in order to assist in data-collection strategy, rather than to determine whether areas will be isomorphous. However, in order to determine if there is a relationship, correlation coefficients of scaled intensities [$CC_1(i, j)$ values output by *XSCALE*; Kabsch, 2010] between data sets collected at different positions for crystals with low and high ratios N were examined. Four data sets were collected from different positions of trypsin ($N = 2.1$) and F_1-ATPase ($N = 14.1$) crystals. For trypsin, all data sets had correlation coefficients above 0.99, indicating a high degree of isomorphism. The F_1-ATPase data sets showed different behaviour. Data sets were collected from three high-intensity positions and one other position. Correlation coefficients between these positions varied from 0.26 between low-intensity and high-intensity positions to 0.96–0.99 for high-intensity positions. While this is a rather limited investigation, it demonstrates that data from crystals with a low ratio N can be merged better than those with a high ratio N. It is also clear that while diffraction varies considerably between positions in F_1-ATPase crystals, some are nevertheless isomorphous. Clustering techniques could then be used to group isomorphous data sets from multiple positions (Foadi *et al.*, 2013; Giordano *et al.*, 2012).

3. Discussion

The ability to measure the extent of crystal variability is an important step in quantifying empirical intra-crystal and inter-crystal variability. As can be seen in Table 1, the values vary greatly between systems, with the most ordered systems studied here maintaining a ratio $N < 10$ and $V_1 < 2$. Obtaining values below this cutoff suggests data-collection strategies that use the full crystal volume, either by using a large beam, translating the crystal during data collection or merging multiple data sets. In the most extreme examples shown here, F_1-ATPase and the small G protein RhoA, the crystals have high
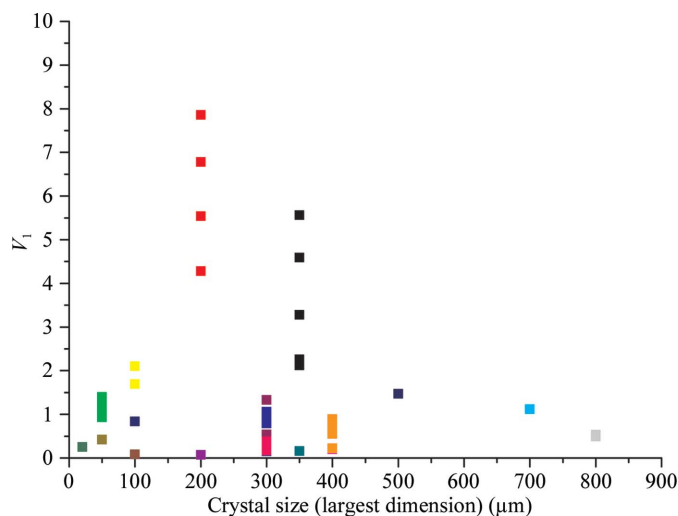
Figure 2
Values of V_1 do not necessarily increase with crystal size. Plot of V_1 values against the largest dimension of the crystal; the colour scheme is the same as in Fig. 1.

values of both V_1 and V_2, the latter showing that parts of the crystals have an intensity ~15 and ~11 times higher than the mean, respectively (Table 1 and Fig. 1). How can these values be used to guide data-collection strategies for these and subsequent crystals? Take F_1-ATPase first. Scanning the crystal with a 7 µm diameter X-ray beam reveals high variability in diffraction intensity, with no contiguous regions. The subsequent strategy will depend on the purpose of the experiment, but the use of a large beam and/or a helical strategy can be ruled out. While RhoA crystals also have high V values, the high-intensity points form a contiguous region approximately 100 µm in diameter. This implies that samples for this project should be scanned to locate the best region, but that a beam diameter of 100 µm would make better use of the diffraction volume, either by changing the beam focus, shaping or using a helical strategy across the optimal volume.

The values obtained also support data-collection strategies that are already used in highly challenging projects. For example, very low values are obtained for a large ribosome crystals ($N = 5.3$), advocating data collection using as much of the crystal volume as possible, the strategy that was used by the Ramakrishnan laboratory when collecting data from these crystals (Clemons *et al.*, 2001), often defocusing the beam. Of particular interest are samples that have a low value of V_1 but a rather high value of V_2, most notably GPCR and pyrophosphatase TVP crystals, both of which are membrane proteins. This situation arises when a crystal contains a very few hot spots that are much higher than the average. Most GPCR crystals have low V values as the intensity is poor throughout the crystals; however, some crystals contain 1–3 regions with much higher intensity. This reflects the experiences of data collection using these crystals, where a large number (often in the thousands) need to be screened and only certain volumes diffract sufficiently using a microfocused beam (Warne *et al.*, 2008). This is also the case with crystals of the membrane-bound pyrophosphatase, where using a microfocused beam was essential to collect data from the most ordered regions of a crystal (Kellosalo *et al.*, 2012). Misleading values are obtained in cases where multiple lattices are present, where low values are obtained as the average intensity is very similar. Here, combination with spot counting or indexing could be used to flag homogeneity arising from multiple lattices. The possibility of estimating the B factor of images would provide an excellent measure of quality that does not possess the problems associated with TIS.

With some care, the value could also be applied between crystals. In this study, separate crystals of insulin and glucose isomerase showed a high level of homogeneity where multiple microcrystals were present on the same support (values of 0.25 and 1.83 for insulin and 0.93 and 3.12 for glucose isomerase for V_1 and V_2 between crystals, respectively). This could be extended to multiple crystals on separate supports, but care would have to be taken in order to collect characterization images using the same resolution and beam intensity. In this way, a measure of the variability between samples could be obtained. With the advent of screening the diffraction properties of crystals in crystallization plates (Jacquamet *et al.*, 2009; Axford *et al.*, 2012), the value could provide an indicator of the level of screening that will be required for a particular project.

With the foreseen increase in the automation of sample evaluation, the values presented here could become one of the measures of quality associated with a sample. The number of samples evaluated at the ESRF and other facilities has been steadily increasing (Bowler *et al.*, 2010), and the advent of pixel-array detectors has enabled many more positions within crystals to be evaluated by reducing data-collection times (Broennimann *et al.*, 2006; Aishima *et al.*, 2010). Sample evaluation on this scale will require additional measures of
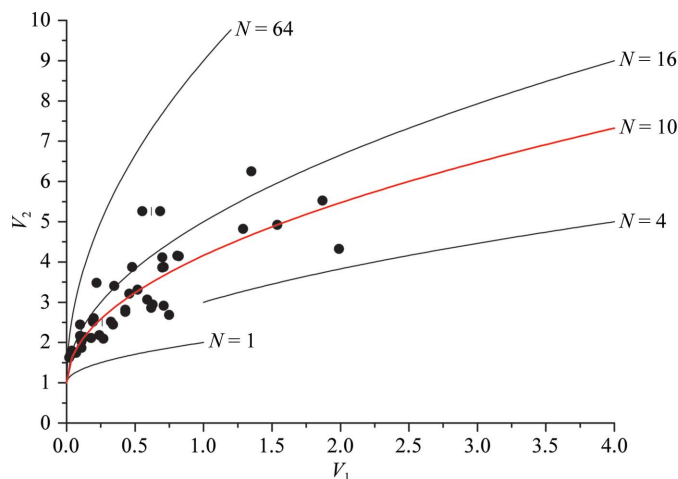

Figure 3
Values observed for users' crystals in the period June to August 2013. Lines show the values obtained for various ratios N between positions at increasing differences in diffraction power.

crystal quality, such as sample variability. The values could then be used, in combination with current indicators of crystal quality, to assist in sample selection and choice of beamline and data-collection strategy. The measures are now calculated for all mesh scans performed on the ESRF Structural Biology beamlines and are stored in the LIMS system ISPyB (Delagenière *et al.*, 2011). The values determined so far are shown in Fig. 3.

References

Aishima, J., Owen, R. L., Axford, D., Shepherd, E., Winter, G., Levik, K., Gibbons, P., Ashton, A. & Evans, G. (2010). *Acta Cryst.* D**66**, 1032–1035.
Axford, D. *et al.* (2012). *Acta Cryst.* D**68**, 592–600.
Baxter, N. J., Bowler, M. W., Alizadeh, T., Cliff, M. J., Hounslow, A. M., Wu, B., Berkowitz, D. B., Williams, N. H., Blackburn, G. M. & Waltho, J. P. (2010). *Proc. Natl Acad. Sci. USA*, **107**, 4555–4560.
Bourenkov, G. P. & Popov, A. N. (2010). *Acta Cryst.* D**66**, 409–419.
Bowler, M. W., Guijarro, M., Petitdemange, S., Baker, I., Svensson, O., Burghammer, M., Mueller-Dieckmann, C., Gordon, E. J., Flot, D., McSweeney, S. M. & Leonard, G. A. (2010). *Acta Cryst.* D**66**, 855–864.
Bowler, M. W., Montgomery, M. G., Leslie, A. G. W. & Walker, J. E. (2006). *Acta Cryst.* D**62**, 991–995.
Brockhauser, S., Svensson, O., Bowler, M. W., Nanao, M., Gordon, E., Leal, R. M. F., Popov, A., Gerring, M., McCarthy, A. A. & Gotz, A. (2012). *Acta Cryst.* D**68**, 975–984.
Broennimann, C., Eikenberry, E. F., Henrich, B., Horisberger, R., Huelsen, G., Pohl, E., Schmitt, B., Schulze-Briese, C., Suzuki, M., Tomizaki, T., Toyokawa, H. & Wagner, A. (2006). *J. Synchrotron Rad.* **13**, 120–130.
Cherezov, V., Hanson, M. A., Griffith, M. T., Hilgart, M. C., Sanishvili, R., Nagarajan, V., Stepanov, S., Fischetti, R. F., Kuhn, P. & Stevens, R. C. (2009). *J. R. Soc. Interface*, **6**, S587–S597.
Clemons, W. M. Jr, Brodersen, D. E., McCutcheon, J. P., May, J. L., Carter, A. P., Morgan-Warren, R. J., Wimberly, B. T. & Ramakrishnan, V. (2001). *J. Mol. Biol.* **310**, 827–843.
Cliff, M. J., Bowler, M. W., Varga, A., Marston, J. P., Szabó, J., Hounslow, A. M., Baxter, N. J., Blackburn, G. M., Vas, M. & Waltho, J. P. (2010). *J. Am. Chem. Soc.* **132**, 6507–6516.

Cusack, S., Belrhali, H., Bram, A., Burghammer, M., Perrakis, A. & Riekel, C. (1998). *Nature Struct. Biol.* **5**, 634–637.

Delagenière, S. *et al.* (2011). *Bioinformatics*, **27**, 3186–3192.

Efremov, R. G., Baradaran, R. & Sazanov, L. A. (2010). *Nature (London)*, **465**, 441–445.

Flot, D., Mairs, T., Giraud, T., Guijarro, M., Lesourd, M., Rey, V., van Brussel, D., Morawe, C., Borel, C., Hignette, O., Chavanne, J., Nurizzo, D., McSweeney, S. & Mitchell, E. (2010). *J. Synchrotron Rad.* **17**, 107–118.

Foadi, J., Aller, P., Alguel, Y., Cameron, A., Axford, D., Owen, R. L., Armour, W., Waterman, D. G., Iwata, S. & Evans, G. (2013). *Acta Cryst.* D**69**, 1617–1632.

Gabadinho, J. *et al.* (2010). *J. Synchrotron Rad.* **17**, 700–707.

Giordano, R., Leal, R. M. F., Bourenkov, G. P., McSweeney, S. & Popov, A. N. (2012). *Acta Cryst.* D**68**, 649–658.

Griffin, J. L., Bowler, M. W., Baxter, N. J., Leigh, K. N., Dannatt, H. R., Hounslow, A. M., Blackburn, G. M., Webster, C. E., Cliff, M. J. & Waltho, J. P. (2012). *Proc. Natl Acad. Sci. USA*, **109**, 6910–6915.

Hilgart, M. C., Sanishvili, R., Ogata, C. M., Becker, M., Venugopalan, N., Stepanov, S., Makarov, O., Smith, J. L. & Fischetti, R. F. (2011). *J. Synchrotron Rad.* **18**, 717–722.

Incardona, M.-F., Bourenkov, G. P., Levik, K., Pieritz, R. A., Popov, A. N. & Svensson, O. (2009). *J. Synchrotron Rad.* **16**, 872–879.

Jacquamet, L., Joly, J., Bertoni, A., Charrault, P., Pirocchi, M., Vernede, X., Bouis, F., Borel, F., Périn, J.-P., Denis, T., Rechatin, J.-L. & Ferrer, J.-L. (2009). *J. Synchrotron Rad.* **16**, 14–21.

Kabsch, W. (2010). *Acta Cryst.* D**66**, 125–132.

Kellosalo, J., Kajander, T., Kogan, K., Pokharel, K. & Goldman, A. (2012). *Science*, **337**, 473–476.

Lutter, R., Abrahams, J. P., van Raaij, M. J., Todd, R. J., Lundqvist, T., Buchanan, S. K., Leslie, A. G. W. & Walker, J. E. (1993). *J. Mol. Biol.* **229**, 787–790.

Mueller-Dieckmann, C., Panjikar, S., Tucker, P. A. & Weiss, M. S. (2005). *Acta Cryst.* D**61**, 1263–1272.

Pellegrini, E., Piano, D. & Bowler, M. W. (2011). *Acta Cryst.* D**67**, 902–906.

Powell, H. R., Johnson, O. & Leslie, A. G. W. (2013). *Acta Cryst.* D**69**, 1195–1203.

Riekel, C., Burghammer, M. & Schertler, G. (2005). *Curr. Opin. Struct. Biol.* **15**, 556–562.

Russi, S., Juers, D. H., Sanchez-Weatherby, J., Pellegrini, E., Mossou, E., Forsyth, V. T., Huet, J., Gobbo, A., Felisaz, F., Moya, R., McSweeney, S. M., Cusack, S., Cipriani, F. & Bowler, M. W. (2011). *J. Struct. Biol.* **175**, 236–243.

Sanchez-Weatherby, J., Bowler, M. W., Huet, J., Gobbo, A., Felisaz, F., Lavault, B., Moya, R., Kadlec, J., Ravelli, R. B. G. & Cipriani, F. (2009). *Acta Cryst.* D**65**, 1237–1246.

Sanishvili, R., Nagarajan, V., Yoder, D., Becker, M., Xu, S., Corcoran, S., Akey, D. L., Smith, J. L. & Fischetti, R. F. (2008). *Acta Cryst.* D**64**, 425–435.

Sauter, N. K., Grosse-Kunstleve, R. W. & Adams, P. D. (2004). *J. Appl. Cryst.* **37**, 399–409.

Selmer, M., Dunham, C. M., Murphy, F. V. IV, Weixlbaumer, A., Petry, S., Kelley, A. C., Weir, J. R. & Ramakrishnan, V. (2006). *Science*, **313**, 1935–1942.

Smith, J. L., Fischetti, R. F. & Yamamoto, M. (2012). *Curr. Opin. Struct. Biol.* **22**, 602–612.

Song, J., Mathew, D., Jacob, S. A., Corbett, L., Moorhead, P. & Soltis, S. M. (2007). *J. Synchrotron Rad.* **14**, 191–195.

Warne, T., Serrano-Vega, M. J., Baker, J. G., Moukhametzianov, R., Edwards, P. C., Henderson, R., Leslie, A. G. W., Tate, C. G. & Schertler, G. F. (2008). *Nature (London)*, **454**, 486–491.

Wheeler, M. J., Russi, S., Bowler, M. G. & Bowler, M. W. (2012). *Acta Cryst.* F**68**, 111–114.

Zhang, Z., Sauter, N. K., van den Bedem, H., Snell, G. & Deacon, A. M. (2006). *J. Appl. Cryst.* **39**, 112–119.